ISSN 2411-3336; e-ISSN 2541-9404

JOURNAL OF MINING INSTITUTE
Zapiski Gornogo instituta
Journal homepage: pmi.spmi.ru



Research article

Mineral composition and thermobarometry of metamorphic rocks of Western Ny Friesland, Svalbard

Yurii L. GULBIN[1], **Sima A. AKBARPURAN KHAIYATI**[1]✉, **Aleksandr N. SIROTKIN**[2]
[1] *Empress Catherine II Saint Petersburg Mining University, Saint Petersburg, Russia*
[2] *Russian Research Institute for Geology and Mineral Resources of the World Ocean named after I.S.Gramberg, Saint Petersburg, Russia*

How to cite this article: Gulbin Yu.L., Akbarpuran Khaiyati S.A., Sirotkin A.N. Mineral composition and thermobarometry of metamorphic rocks of Western Ny Friesland, Svalbard. Journal of Mining Institute. 2023. Vol. 263, p. 657-673. EDN XGNKDQ

Abstract. The results of the study of mineral composition and microstructure of representative metapelitic and calcic pelitic schist and amphibole-biotite gneiss, occurring in the northern part of the Western Ny Friesland anticlinorium, are reported. Mineral composition was analyzed with a JSM-6510LA scanning electron microscope with a JED-2200 (JEOL) energy dispersive spectrometer. Metamorphic conditions were assessed with various mineral geothermometers (garnet-biotite, Ti-in-biotite, Ti-in-muscovite, Ti-in-amphibole, garnet-amphibole, amphibole-plagioclase, and chlorite) and geothermobarometers (GASP, GBPQ, GRIPS, GBPQ, phengite, etc.). It has been shown that peak temperature and pressure for rocks of the Paleoproterozoic Atomfjella Series forming the western limb of the anticlinorium are consistent with those for the high-pressure part of the upper amphibolite facies (690-720 °C, 9-12 kbar), and the peak temperature and pressure for rocks of the Mossel Series occurring in the eastern limb and rest on the Atomfjella rock sequence, are consistent with the high-pressure part of the lower amphibolite facies (580-600 °C, 9-11 kbar). In addition to the high-temperature parageneses Ms-Bt-Grt-Pl (±Ky, St), Bt-Grt-Pl-Kfs-Cal (±Scp) and Bt-Hbl-Ep-Grt-Pl, the rocks of the both series display the low-temperature assemblage Ms-Chl-Ep-Ab-Prh-Ttn, which was formed upon transition from greenschist to prehnite-pumpellyite facies (260-370 °C).

***Keywords*:** metapelitic and calcic pelitic schist; amphibole-biotite gneiss; mineral thermobarometry; conditions of metamorphism; Ny Friesland; Svalbard

Received: 30.03.2023 ***Accepted: 20.09.2023*** ***Online: 27.10.2023*** ***Published: 27.10.2023***

Introduction. The distinctive geological structure of Svalbard [1-3] and adjacent territories [4-6] has been the subject of long debate [7-9] due to the tectonic position of the archipelago, which is located on the northwestern Barents-Kara continental margin [10] at the Svalbard Plate – North Atlantic contact. Being part of a formerly integrated fold belt, which formed completely in Middle Devonian time, Svalbard crystalline complexes, together with the Caledonides in the northern Appalachians, Eastern Greenland, the British Isles, and Scandinavia, are interpreted as fragments projecting now on both sides of the ocean. The tectonics and rock composition of the above complexes are studied to reconstruct the sequence of tectonothermal events responsible for the geological evolution of the region [11-13].

Geological background. Occurring at the base of Western Ny Friesland are metamorphic rock complexes (Fig.1) forming a large-scale geologic structure interpreted as a near N-S trending, ~ 150 km long anticlinorium. Its axis spatially coincides with a deep long-lived fault. The core of the anticlinorium is exposed on northern Mossel Peninsula. Its western limb consists of volcanic-sedimentary rocks making up the Paleoproterozoic (~1750 Ma) Atomfjella Series. Atomfjella rocks

This is an open access article under the CC BY 4.0 license

© Yurii L. Gulbin, Sima A. Akbarpuran Khaiyati, Aleksandr N. Sirotkin, 2023

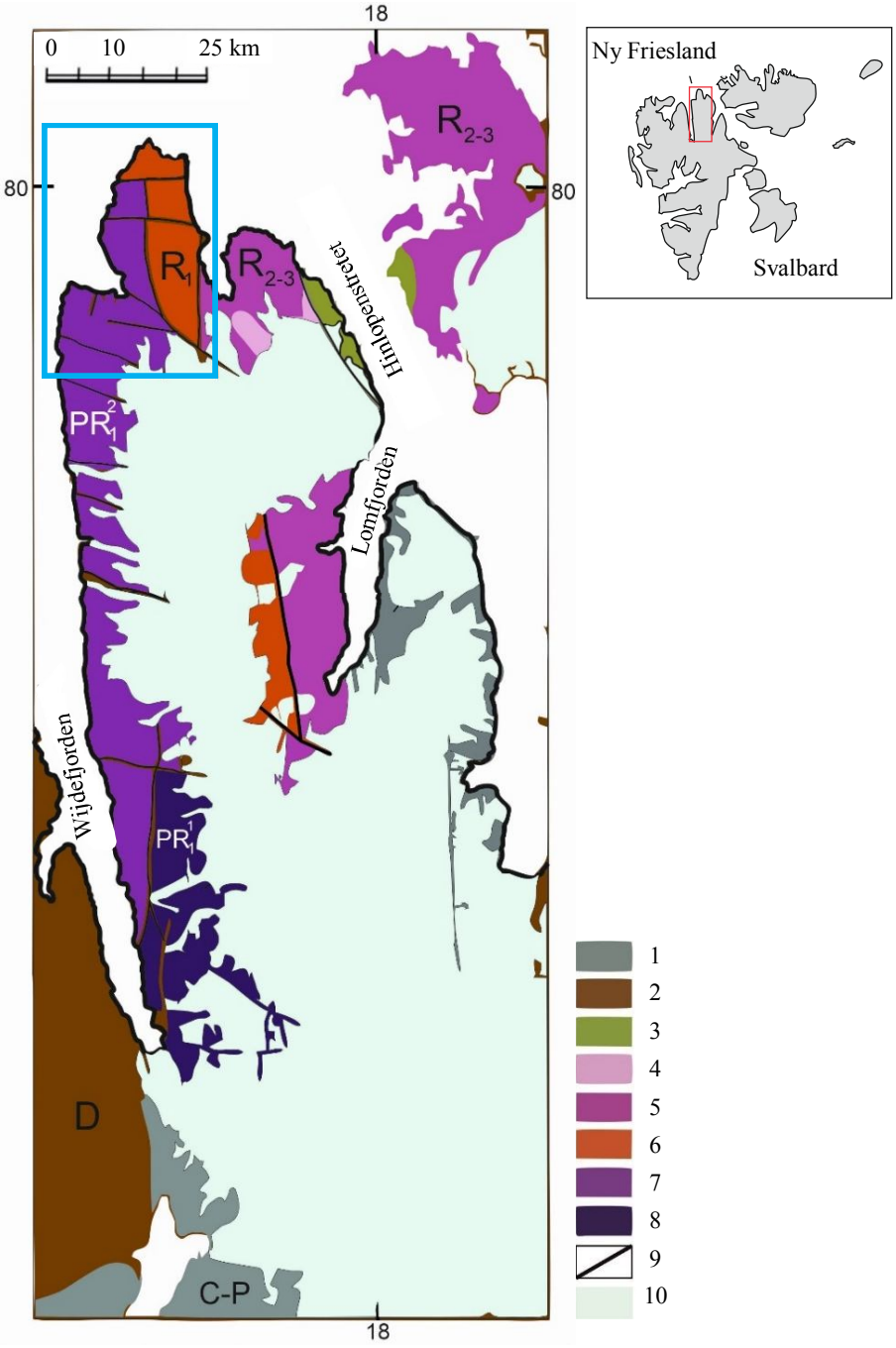


Fig.1. Geological sketch map of Ny Friesland Peninsula [14, simplified]

1 – platform rock sequences (PZ_1); 2 – terrigenous complex (D); 3 – Oslobreen Series (Є-O); 4 – Polarisbreen Series (V); 5 – Lomfjorden Series (RF_3); 6 – Mossel Series (RF_1); 7, 8 – Atomfjella Series (PR_1): 7 – upper subseries, 8 – lower subseries; 9 – tectonic dislocations; 10 – ice cover. The study area is delineated with a blue frame

(gneisses, often migmatized, schists, quartzites and marbles) are thrown into isoclinals folds with low-angle thrusts. The sequence is cut by small anatectic granite bodies and meta-ultramafic and meta-gabbroic rock intrusions. Within the eastern limb, it is overlain with structural unconformity by Lower and Middle Riphean Mossel sediments. These rocks (schists and gneisses with quartzite and marble interbeds) form a steep monocline, which dips east and displays small open folds. The eastern boundary of the anticlinorium is indicated by the tectonic contact of the Mossel Series with the Upper Riphean Lomfjord Series, in which rocks are poorly metamorphosed, making up the western limb of the Hinlopen synclinorium.

This is an open access article under the CC BY 4.0 license

Journal of Mining Institute. 2023. Vol. 263. P. 657-673
© Yurii L. Gulbin, Sima A. Akbarpuran Khaiyati, Aleksandr N. Sirotkin, 2023

Aim of studies. The region's geology has been studied by the Polar Marine Geological Prospecting Survey. A 1:100000-scale geologic map for the northern part of the peninsula, based on the results of geological survey, was compiled and the composition of Western Ny Friesland crystalline complexes was described. The aim of a new stage of studies is to assess the age, the temperatures, pressures and geodynamic setting of metamorphism. The primary goals of our efforts are the detail petrography, studying composition of minerals and estimation of *P-T*-parameters of metamorphism.

Methods. Representative rock samples from the Atomfjella and Mossel series, taken from the northern zone of the anticlinorium, were analyzed. In petrographic studies, attention was focused on the microstructure of the rocks and relationships between minerals. Their composition was analyzed by a JSM-6510LA scanning electron microscope equipped with a JED-2200 (JEOL) energy dispersive spectrometer. Metamorphic conditions were estimated using mineral thermobarometry. The representative compositions of the minerals used for thermobarometric calculations are shown in Table 1.

Petrography and mineral chemistry. The samples analyzed were divided into three groups: metapelitic schists consisting of the Ms-Bt-Grt-Pl (±Ky, St) assemblage (symbols of minerals are given after [15]); calcic pelitic schists, which also contains calcite, scapolite, epidote-group minerals, titanite, and K-feldspar; amphibole-biotite plagiogneisses.

Atomfjella Series. Rittervatnet Suite. Metapelitic schist 3912-3a

• Petrography. The rock contains Qz (35-40 vol.%), Ms (40-35 vol.%), Grt (12-14 vol.%), Bt (4-5 vol.%), Pl (4-3 vol.%), Ilm (2-1 vol.%), Chl (2-1 vol.%), Tur (1 vol.%), Ky, Kfs, carbonaceous matter (< 1 vol.%). Apatite, zircon, rutile, monazite-(Ce), allanite-(Ce) and hydroxylbastnesite-(Ce) are present as accessories. The rock matrix consists of granoblastic quartz and plagioclase grains, lamellar crystals of muscovite (up to 1 mm in size) and subordinate biotite, and scarce kyanite (Fig.2, *a*). Carbonaceous matter occurs in mica crystal interstices (Fig.2, *b*). Garnet forms porphyroblasts with *S*-shaped tails of quartz and other matrix mineral inclusions. Garnet porphyroblasts often display a fancy structure, which is due to an abundance of quartz inclusions (Fig.2, *c*). The distribution of ore mineral inclusions shows a zonal pattern: ilmenite is replaced by rutile from core to rim of the porphyroblasts [16].

Garnet crystals are surrounded by the biotite-muscovite aggregate (Fig.2, *c*), suggesting syntectonic porphyroblastesis. Late mineralization occurs as lenticular chlorite and sericitized plagioclase aggregates in the matrix, chlorite-albite-K-feldspar micro-veinlets with plates of carbonaceous matter cross-cutting garnet (Fig.2, *d-f*), and hydroxybastnesite-(Ce) rims around allanite crystals (Fig.2, *g*).

• Mineral chemistry. Plagioclase from the matrix is oligoclase and shows zoning: from core to rim, the An end-member mole fraction increases from 0.14 to 0.21 (Fig.2, *h*, *i*). It was subjected locally to late albitization. The composition of plagioclase from inclusions in garnet varies from oligoclase (An_{20}) to andesine (An_{32-34}). Muscovite is treated as quaternary solid solution of muscovite, paragonite, Mg-celadonite, and Fe-celadonite end members [17]. Si concentration in white mica varies from 2.98-3.11 atom per formula units (apfu) (in contact with garnet) to 3.04-3.17 apfu (in the matrix), Mg content reaches 0.16 apfu and Fe content reaches 0.09 apfu. White mica is enriched in titanium (TiO_2 0.3-1.1 wt.%). Biotite is also enriched in titanium (TiO_2 2.0-3.2 wt.%), displays moderate Mg content [Mg# = Mg/(Mg + Fe) = 0.46-0.50] and elevated alumina content (Al_2O_3 19-20 wt.%, Al 1.7-1.8 apfu). Chlorite is rich in Fe [Fe# = Fe/(Mg + Fe) = 0.68-89] and poor in Si (2.5-2.7 apfu). In Hey's diagram (Hey M.H. A new review of chlorite. Mineralogical Magazine. 1954. Vol. 30, p. 277-292), chlorite plots the ripidolite field. Al content in chlorite is high (2.7-2.9 apfu) with close ratios of Al^{IV} and Al^{VI}. The degree of filling of octahedral positions (R^{VI}) is 5.8-6.0 apfu.

This is an open access article under the CC BY 4.0 license

This is an open access article under the CC BY 4.0 license

Journal of Mining Institute. 2023. Vol. 263. P. 657-673

© Yurii L. Gulbin, Sima A. Akbarpuran Khaiyati, Aleksandr N. Sirotkin, 2023

EDN XGNKDQ

Table 1

Mineral chemistry (wt.%) used for thermobarometry

Series	Atomfjella																	
Sample	3912-3a						3912-3b					4072-2						
Mineral	Grt	Bt	Bt	Pl	Ms	Ms	Grt	Bt	Bt	Pl	Ms	Grt	Grt	Bt	Pl	Pl	Ms	Ms
Analysis	001	068	077	070	066	075	034	069	022	070	075	025	028	006	061	079	062	071
Position	r	r	m	m	r	m	r	m	r	m	m	r	r	m	m	m	m	m
SiO_2	37.48	35.10	35.08	61.64	44.85	46.26	36.78	36.09	33.42	46.48	46.18	36.65	36.82	33.74	46.17	55.88	47.04	48.19
TiO_2	0.00	1.94	3.01	0.00	0.49	1.10	0.00	2.88	0.89	0.00	0.00	0.00	0.00	4.24	0.00	0.00	0.00	0.79
Al_2O_3	21.42	19.91	19.24	23.87	35.47	33.91	21.08	16.78	19.06	34.77	35.87	20.79	21.52	16.80	34.18	27.85	35.43	31.60
FeO*	32.17	18.43	18.62	0.19	1.23	1.18	27.05	17.87	23.38	0.00	0.42	29.85	28.25	26.63	0.22	0.00	0.81	2.28
MnO	0.00	0.00	0.00	0.00	0.00	0.00	2.03	0.09	0.26	0.00	0.09	0.19	0.16	0.00	0.00	0.00	0.00	0.00
MgO	4.04	9.58	9.47	0.00	0.78	1.12	2.48	11.95	9.07	0.00	0.56	1.62	1.45	7.16	0.00	0.00	0.00	0.89
CaO	4.51	0.00	0.00	4.33	0.00	0.00	9.69	0.00	0.00	16.47	0.00	9.82	10.96	0.00	16.60	9.86	0.00	0.00
Na_2O	0.00	0.29	0.29	9.09	0.75	0.83	0.00	0.29	0.00	1.99	0.00	0.00	0.00	0.06	2.10	5.72	0.47	0.63
K_2O	0.00	9.13	9.41	0.04	10.15	10.08	0.00	9.23	7.80	0.18	10.97	0.00	0.00	9.46	0.10	0.19	11.86	10.74
Sum	99.62	94.39	95.12	99.17	93.72	94.48	99.11	94.90	93.89	99.89	94.11	98.92	99.16	94.64	99.37	99.50	94.95	95.12
Crystallochemical coefficients																		
Si	2.986	2.679	2.667	2.753	3.035	3.102	2.957	2.740	2.623	2.136	3.096	2.969	2.958	2.678	2.137	2.522	3.136	3.230
Ti	0.000	0.112	0.172	0.000	0.025	0.055	0.000	0.165	0.053	0.000	0.000	0.000	0.000	0.240	0.000	0.000	0.000	0.040
Al	2.012	1.791	1.725	1.257	2.830	2.681	1.998	1.501	1.763	1.883	2.835	1.985	2.038	1.488	1.865	1.482	2.784	2.496
Fe	2.144	1.177	1.184	0.007	0.069	0.066	1.819	1.134	1.535	0.000	0.024	2.023	1.898	1.673	0.000	0.000	0.043	0.128
Mn	0.000	0.000	0.000	0.000	0.000	0.000	0.138	0.006	0.017	0.000	0.005	0.013	0.011	0.000	0.000	0.000	0.000	0.000
Mg	0.480	1.090	1.074	0.000	0.078	0.112	0.297	1.352	1.061	0.000	0.056	0.196	0.173	0.802	0.000	0.000	0.000	0.089
Ca	0.385	0.000	0.000	0.207	0.000	0.000	0.835	0.000	0.000	0.811	0.000	0.853	0.943	0.000	0.823	0.477	0.000	0.000
Na	0.000	0.043	0.042	0.787	0.098	0.108	0.000	0.000	0.000	0.177	0.000	0.000	0.000	0.009	0.188	0.501	0.058	0.082
K	0.000	0.889	0.913	0.002	0.876	0.863	0.000	0.894	0.881	0.011	0.939	0.000	0.000	0.907	0.006	0.011	0.958	0.918
Sum	8.008	7.868	7.776	5.014	7.012	6.987	8.044	7.792	7.833	5.017	6.956	8.039	8.023	7.796	5.028	4.993	6.979	6.983

End of Table 1

Series	Atomfjella							Mossel																
Sample	4143-1							3885-1							4032-1									
Mineral	Grt	Grt	Hbl	Hbl	Hbl	Bt	Pl	Grt	Grt	Bt	Bt	Pl	Pl	Ms	Grt	Grt	Grt	Bt	Bt	Bt	Pl	Pl	Ms	Ms
Analysis	001	084	041	101	102	046	016	001	033	063	067	024	050	068	001	010	025	032	034	053	014	037	034	046
Position	r	r	m	m	m	m	m	r	r	m	m	r	m	m	r	r	r	r	r	m	r	m	r	m
SiO_2	36.91	37.38	41.50	40.23	40.61	35.52	57.58	36.64	37.35	35.73	8.5	64.25	64.50	46.85	37.32	36.24	36.52	34.97	36.30	35.86	63.82	63.01	45.41	45.86
TiO_2	0.00	0.00	0.82	1.15	0.68	2.95	0.00	0.00	0.00	1.47	1.44	0.00	0.00	0.29	0.00	0.00	0.00	1.22	1.21	1.58	0.00	0.00	0.37	0.50
Al_2O_3	21.05	20.75	13.67	14.46	13.88	15.83	26.23	21.66	21.24	20.00	19.08	22.50	22.20	34.96	21.47	21.02	21.31	19.24	19.80	18.66	22.95	22.93	36.86	35.87
FeO*	30.27	30.50	16.50	17.10	18.59	19.92	0.00	35.87	35.14	18.18	17.69	0.00	0.00	1.26	34.16	36.01	35.90	21.05	18.79	18.65	0.30	0.00	1.18	1.11
MnO	0.58	0.62	0.18	0.32	0.23	0.29	0.00	0.00	0.00	0.00	0.00	0.00	0.00	0.00	0.06	0.10	0.07	0.01	0.00	0.00	0.00	0.00	0.00	0.00
MgO	3.55	4.11	9.50	8.83	7.88	11.47	0.00	3.63	3.49	10.88	11.21	0.00	0.00	1.03	2.16	2.46	2.86	9.88	10.28	10.73	0.00	0.00	0.59	0.74
CaO	6.99	6.16	11.29	11.69	11.87	0.00	8.42	1.66	2.54	0.00	0.00	2.87	3.06	0.00	4.83	3.13	2.59	0.00	0.00	0.00	3.09	2.89	0.00	0.00
Na_2O	0.00	0.00	1.07	1.10	0.91	0.09	7.18	0.00	0.00	0.00	0.30	9.75	9.86	1.56	0.00	0.00	0.00	0.23	0.00	0.00	9.20	9.94	1.78	1.69
K_2O	0.00	0.00	0.57	0.83	0.83	8.84	0.19	0.00	0.00	7.76	8.54	0.00	0.10	8.73	0.00	0.00	0.00	8.57	9.25	9.42	0.07	0.11	8.83	8.95
Sum	99.36	99.52	95.10	95.71	95.46	95.02	99.91	99.45	99.77	94.01	94.23	99.37	99.72	94.69	99.21	98.96	99.24	95.16	95.63	94.90	99.43	98.87	95.01	94.72
Crystallochemical coefficients																								
Si	2.960	2.986	6.249	6.090	6.214	2.734	2.589	2.956	2.997	2.704	2.727	2.843	2.848	3.111	2.993	2.961	2.965	2.675	2.728	2.726	2.825	2.811	3.013	3.052
Ti	0.000	0.000	0.093	0.131	0.078	0.170	0.000	0.000	0.000	0.083	0.082	0.000	0.000	0.015	0.000	0.000	0.000	0.070	0.069	0.090	0.000	0.000	0.018	0.025
Al	1.990	1.954	2.425	2.581	2.503	1.431	1.390	2.060	2.009	1.783	1.705	1.173	1.155	2.737	2.030	2.024	2.039	1.735	1.754	1.673	1.197	1.205	2.883	2.814
Fe	2.030	2.038	2.078	2.164	2.379	1.278	0.011	2.420	2.358	1.150	1.121	0.000	0.000	0.070	2.291	2.460	2.437	1.347	1.181	1.186	0.011	0.000	0.065	0.062
Mn	0.039	0.042	0.023	0.041	0.030	0.019	0.000	0.000	0.000	0.000	0.000	0.000	0.000	0.000	0.004	0.007	0.005	0.001	0.000	0.000	0.000	0.000	0.000	0.000
Mg	0.424	0.489	2.132	1.994	1.796	1.311	0.000	0.436	0.417	1.226	1.267	0.000	0.000	0.102	0.258	0.300	0.346	1.126	1.152	1.216	0.000	0.000	0.058	0.073
Ca	0.601	0.527	1.821	1.896	1.946	0.000	0.406	0.143	0.219	0.000	0.000	0.136	0.145	0.000	0.415	0.274	0.225	0.000	0.000	0.000	0.147	0.138	0.000	0.000
Na	0.000	0.000	0.314	0.323	0.269	0.013	0.626	0.000	0.000	0.000	0.044	0.836	0.845	0.201	0.000	0.000	0.000	0.034	0.000	0.000	0.789	0.859	0.229	0.218
K	0.000	0.000	0.110	0.161	0.162	0.865	0.011	0.000	0.000	0.749	0.826	0.000	0.006	0.740	0.000	0.000	0.000	0.836	0.887	0.914	0.004	0.006	0.747	0.760
Sum	8.045	8.037	15.245	15.380	15.377	7.819	5.034	8.015	7.999	7.696	7.773	4.989	4.999	6.976	7.992	8.027	8.016	7.823	7.770	7.804	4.973	5.020	7.015	7.004

Notes. Atom per formula units (apfu) are based on 12O (garnet), 11O (biotite, muscovite), 13($C + T$) amphibole, 8O (plagioclase). FeO* – total iron. 0.00 – component concentration below the detection limit. Location: m – matrix, r – crystal rim (garnet), contact with garnet (biotite and muscovite).

This is an open access article under the CC BY 4.0 license

© Yurii L. Gulbin, Sima A. Akbarpuran Khaiyati, Aleksandr N. Sirotkin, 2023

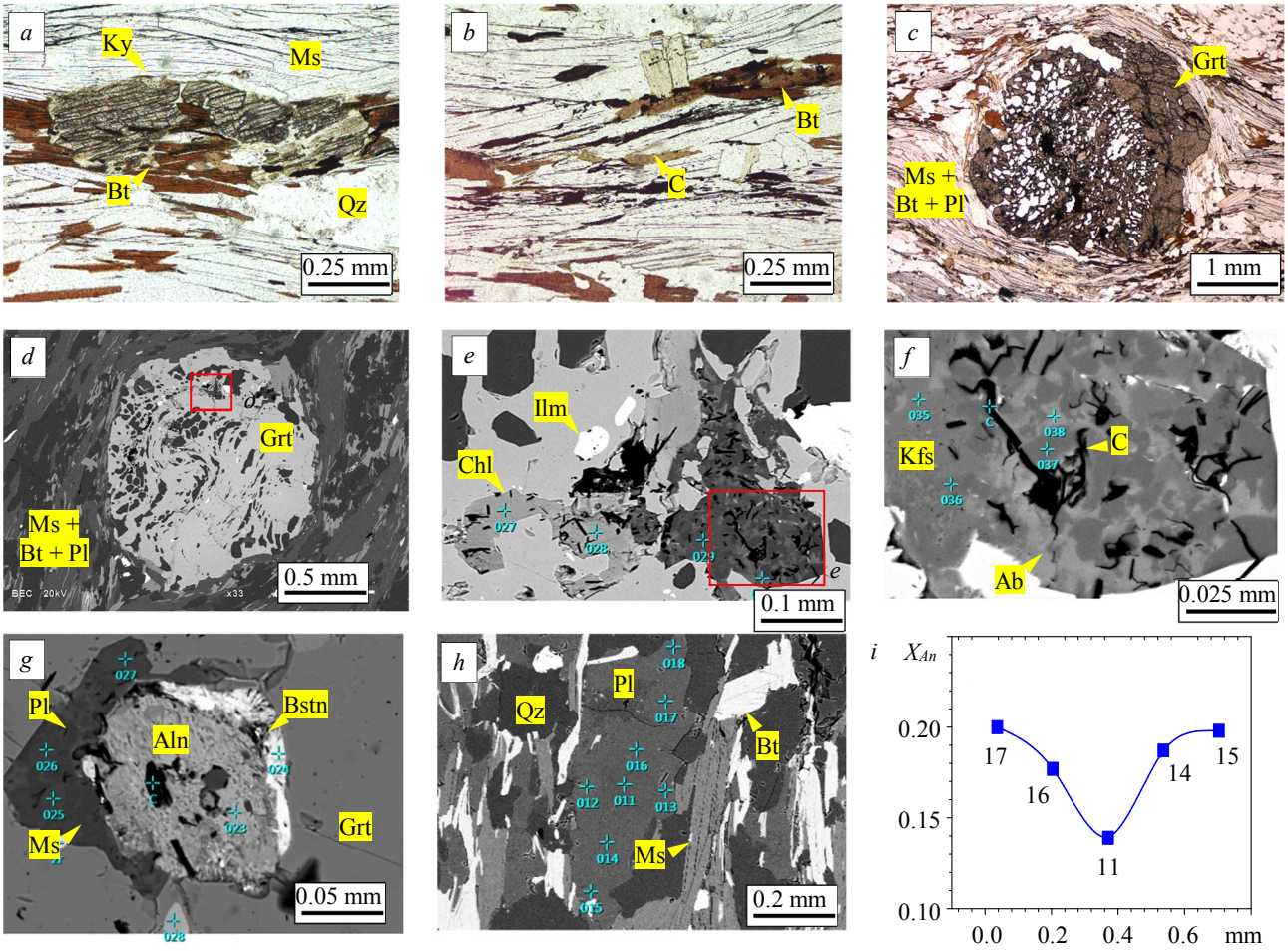


Fig.2. Relationships between minerals in metapelitic schist. Sample 3912-3a. Images in transmitted light, without analyzer (*a-c*) and in back-scattered electrons (*d-h*): *a* – kyanite crystal in quartz-plagioclase-mica matrix; *b* – carbonaceous matter in the interstices of muscovite plates; *c, d* – garnet porphyroblasts with *S*-shaped trails of inclusions surrounded with quartz-plagioclase-mica aggregate; *e, f* – close-up of fragments of chlorite and albite-K-feldspar micro-veinlets with plates of carbonaceous matter in garnet (*d*); *g* – hydroxylbastnesite-(Ce) (Bstn) rim around allanite-(Ce) inclusion in garnet; *h, i* – plagioclase crystal and the concentration profile with analytical points

Garnet is generally enriched in the grossular end member (X_{Ca} 0.12-0.14) and exhibits growth zoning: mole fractions of spessartine and almandine end members decrease from core to rim (X_{Mn} ranges between 0.05-0.06 and 0.01, X_{Fe} between 0.80-0.81 and 0.74-0.75). Hence, the mole fraction of the pyrope end member increases between 0.04-0.05 and 0.14-0.16.

The composition of REE- and Ti-bearing accessory minerals (monazite, allanite, and ilmenite) was discussed in [16]. Hydroxybastnesite, which overgrowth allanite, inherits its compositional characteristics: at ΣREE content of 0.60-0.68 apfu, Ca 0.16-0.32 apfu, and F 0.12-0.21 apfu (O = 1.5), it shows the prevalence of Ce (0.26-0.29 apfu), Nd (0.18-0.19 apfu) and La (0.13-0.15 apfu) over Pr and Sm (0.01-0.04 apfu); its ThO_2 content increases to 3.3 wt.%.

Calcic pelitic schist 3912-3b

• Petrography. The rock contains Qz (15-20 vol.%), Kfs (20-15 vol.%), Ms + Ser (20-15 vol.%), Bt (15-10 vol.%), Cal (11-8 vol.%), Grt (7-10 vol.%), Scp (5-10 vol.%), Pl (4-7 vol.%), Chl (2-4 vol.%), Ttn (1 vol.%), Czo, Ep, Ilm, Rt (< 1 vol.%). Apatite, zircon, and allanite-(Ce) are present as accessories. The rock has a finely banded structure produced by the alternation of lenticular interlayers enriched in sericitized plagioclase and biotite, quartz and K-feldspar, and calcite and scapolite (Fig.3, *a-e*). The latter forms irregular monocrystalline aggregates, up to 1-2 mm in size, which replace biotite (Fig.3, *f*).

This is an open access article under the CC BY 4.0 license

Journal of Mining Institute. 2023. Vol. 263. P. 657-673
© Yurii L. Gulbin, Sima A. Akbarpuran Khaiyati, Aleksandr N. Sirotkin, 2023

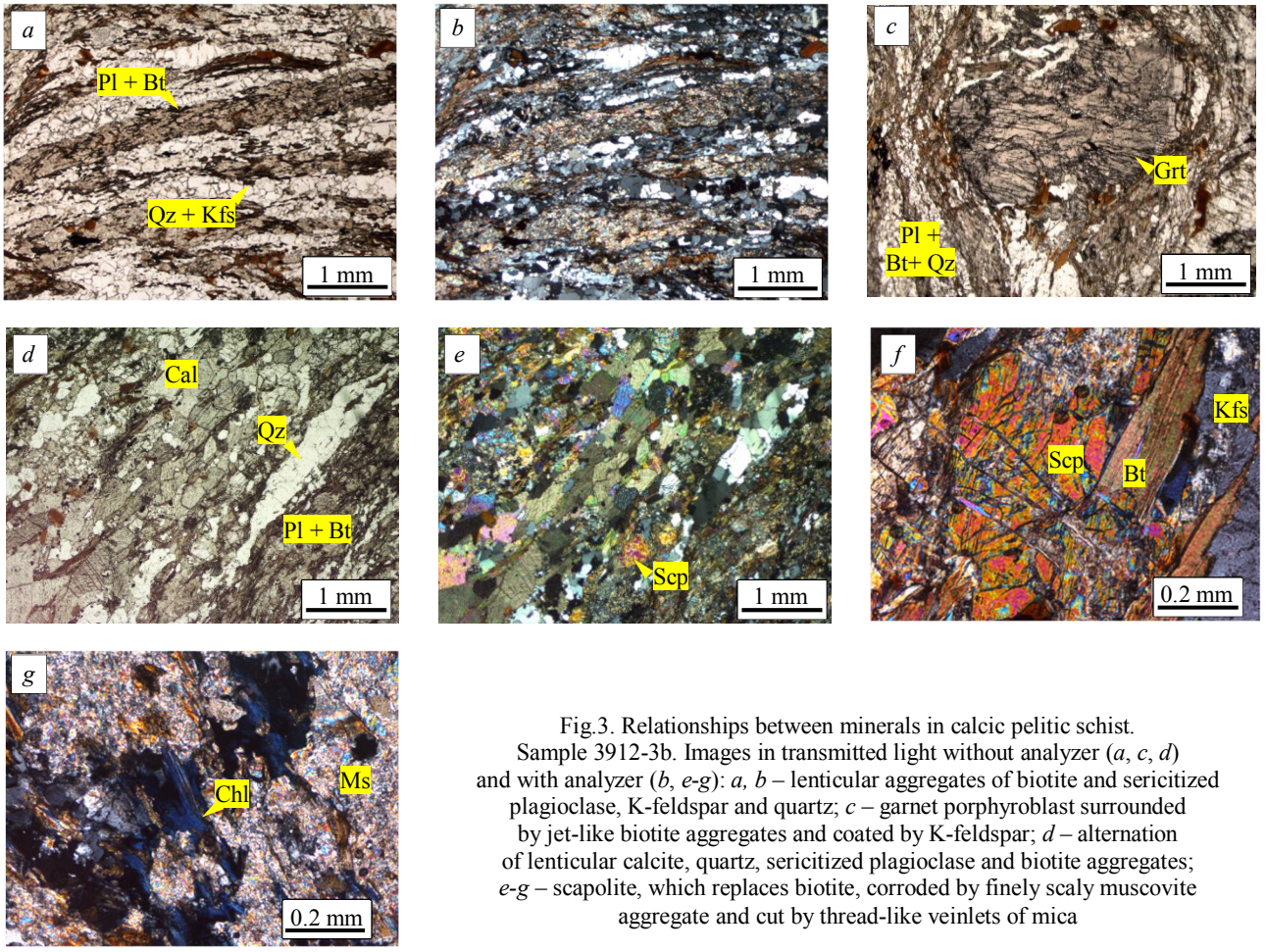


Fig.3. Relationships between minerals in calcic pelitic schist. Sample 3912-3b. Images in transmitted light without analyzer (*a*, *c*, *d*) and with analyzer (*b*, *e-g*): *a, b* – lenticular aggregates of biotite and sericitized plagioclase, K-feldspar and quartz; *c* – garnet porphyroblast surrounded by jet-like biotite aggregates and coated by K-feldspar; *d* – alternation of lenticular calcite, quartz, sericitized plagioclase and biotite aggregates; *e-g* – scapolite, which replaces biotite, corroded by finely scaly muscovite aggregate and cut by thread-like veinlets of mica

Garnet occurs as isometric porphyroblasts, up to 1 cm in size, surrounded by matrix layers and jet-like biotite aggregates. They have lenticular «coating» consisting of K-feldspar (Fig.3, *c*). The porphyroblasts contain quartz, K-feldspar, plagioclase, biotite, and ilmenite inclusions, and are cut by thread-like veinlets of chlorite, clinozoisite, epidote, late K-feldspar, and calcite.

Ilmenite is often intergrown with rutile and overgrown with rims of titanite, which also evolve along cleavage cracks in chlorite. Accessory allanite is closely intergrown with REE-bearing clinozoisite, forming crystal cores with external zones consisting of clinozoisite [16].

The rock typically shows an abundance of the late chlorite-muscovite assemblage. Finely scaly mica aggregates replace plagioclase, biotite, and scapolite, and are cut by micro-veinlets of chlorite (Fig.3, *f, g*).

Mineral chemistry. Plagioclase from inclusions in garnet is andesine-labradorite (An_{42-52}), while plagioclase in the matrix is more anorthitic (bytownite, An_{82}). Scapolite is sodium meionite (mizzonite) $Ca_3NaAl_5Si_7O_{24}CO_3$ [18], as indicated by averaged chemical formula of the mineral (n = 5): $(Ca_{2,94\text{-}3,06}Na_{0,82\text{-}0,91})_{3,80\text{-}4,01}(Al_{5,11\text{-}4,99}Si_{6,90\text{-}7,01})_{12}O_{24}(CO_3)_{0,84\text{-}1,05}$. K-feldspar contains minor Na_2O (0.4-0.8 wt.%, X_{Na} 0.05-0.07) and BaO (up to 1.7 wt.%). Calcite contains minor FeO (up to 2.6 wt.%), MgO (up to 1.7 wt.%), and MnO (up to 1.9 wt.%). Muscovite is enriched in Si (3.06-3.16 apfu), Mg (up to 0.11 apfu), Fe (up to 0.07 apfu) and depleted in TiO_2 (< 0.1 wt.%). White mica occasionally contains up to 1.9 wt.% BaO. Biotite has low Al_2O_3 (16-17 wt.%, Al 1.45-1.50 apfu), moderate MgO (Mg# 0.39-0.54), and elevated TiO_2 (2.9-3.4 wt.%). Chlorite is similar in composition to chlorite from sample 3912-3a. Garnet is enriched in the grossular end member (X_{Ca} 0.26-0.28) and shows normal Fe, Mg, and Mn zoning (core: X_{Fe} 0.63-0.64, X_{Mn} 0.06-0.07, X_{Mg} 0.04; rim: X_{Fe} 0.60-0.61, X_{Mn} 0.04, X_{Mg} 0.09-0.10). The chemical composition of accessory minerals was described in the previous publication of the authors [16].

This is an open access article under the CC BY 4.0 license

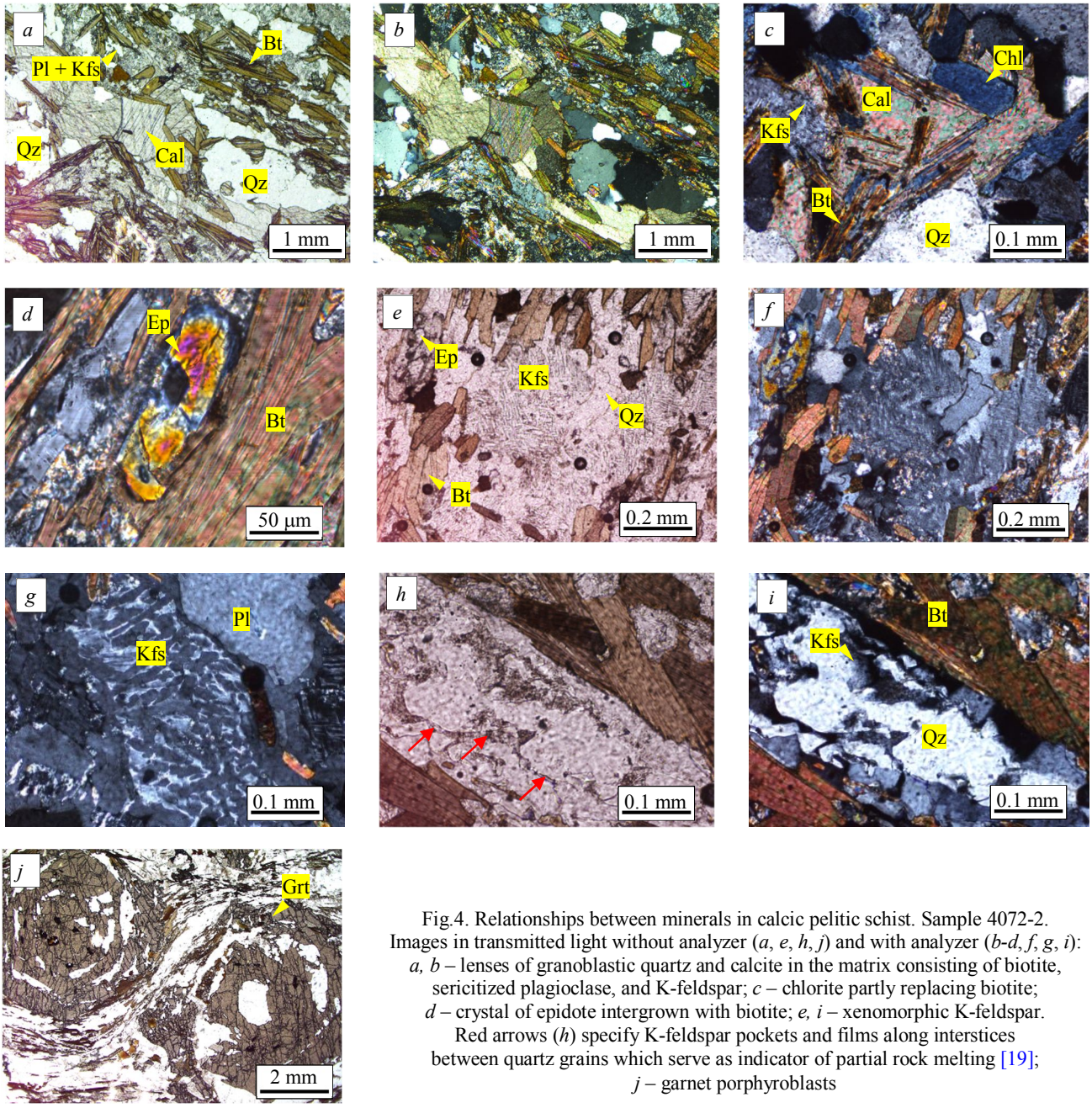


Fig.4. Relationships between minerals in calcic pelitic schist. Sample 4072-2. Images in transmitted light without analyzer (*a*, *e*, *h*, *j*) and with analyzer (*b-d*, *f*, *g*, *i*): *a, b* – lenses of granoblastic quartz and calcite in the matrix consisting of biotite, sericitized plagioclase, and K-feldspar; *c* – chlorite partly replacing biotite; *d* – crystal of epidote intergrown with biotite; *e, i* – xenomorphic K-feldspar. Red arrows (*h*) specify K-feldspar pockets and films along interstices between quartz grains which serve as indicator of partial rock melting [19]; *j* – garnet porphyroblasts

Calcic pelitic schist 4072-2

• Petrography. The rock contains Qz (25-30 vol.%), Ms + Ser (25-20 vol.%), Kfs (10-15 vol.%), Bt (9-10 vol.%), Grt (8-9 vol.%), Cal (10-5 vol.%), Pl (7-5 vol.%), Chl (4-2 vol.%), Ttn (1-2 vol.%), Ilm (1-2 vol.%), Ep, Prh (< 1 vol.%). Apatite, magnetite and zircon are present as accessories. The rock shows a crenulated structure. It consists of lens-shaped aggregates of biotite, sericitized plagioclase, and prehnite, which alternate with lenses of granoblastic quartz and calcite (Fig.4, *a, b*). Biotite is often finely intergrown with muscovite and is partly replaced by chlorite (Fig.4, *c*). Also spatially associated with biotite are fine (0.1 mm) prismatic epidote crystals oriented along schistosity (Fig.4, *d*) and xenomorphic mesoperthitic K-feldspar (Fig.4, *e-i*). The matrix contains scattered ~0.6 mm thick idiomorphic titanite crystals and plate ilmenite grains of various sizes (0.1-0.5 mm); these minerals are often intergrown.

Garnet forms coarse (up to 5-7 mm) isometric crystals surrounded by biotite and having concentric zoning caused by the presence of arcuate fragments in the rims of porphyroblasts

This is an open access article under the CC BY 4.0 license

Journal of Mining Institute. 2023. Vol. 263. P. 657-673
© Yurii L. Gulbin, Sima A. Akbarpuran Khaiyati, Aleksandr N. Sirotkin, 2023

separated from their cores by quartz interlayers (Fig.4, *j*). The porphyroblasts often contain concentric tails of biotite, epidote, and ilmenite inclusions.

• Mineral chemistry. Plagioclase varies in composition from andesine to bytownite (An_{49-81}). K-feldspar contains minor Na_2O (0.7-0.9 wt.%). Calcite contains minor FeO (up to 3.1 wt.%), MgO (up to 1.3 wt.%), and MnO (up to 0.5 wt.%). The Fe^{3+} content in epidote varies between 0.57 and 0.78 apfu. Epidote crystals often show zoning produced by appearance of Fe-depleted rims at their margins. Prehnite occurs as an iron-bearing variety: $Ca_{1.92-1.93}(Al_{0.89-0.90}Fe_{0.18-0.19})_{1.07-1.09}(Al_{1.02-0.98}Si_{2.98-3.02})O_{10}(OH)_2$ ($n = 2$). Muscovite is markedly enriched in Si (3.11-3.23 apfu), Mg (up to 0.11 apfu), and Fe (up to 0.13 apfu); also, it contains TiO_2 (up to 0.8 wt.%). Biotite is poor in Al_2O_3 (15-16 wt.%, Al 1,4-1,5 apfu) and MgO (Mg# 0.31-0.33) but is rich in TiO_2 (4.1-4.7 wt.%). Garnet shows the high content of Ca which increase from core (X_{Ca} 0.22) to rim (X_{Ca} 0.31). Also it has Mg and Mn growth zoning (core: X_{Mg} 0.04, X_{Mn} 0.04; rim: X_{Mg} 0.06, X_{Mn} 0.004). Ilmenite has the low MnO content (< 0.8 wt.%). Magnetite contains minor TiO_2 (1.2 wt.%), V_2O_5 (1.2 wt.%), and Cr_2O_3 (0.4 wt.%).

Amphibole-biotite plagiogneiss 4143-1

• Petrography. The rock contains Qz (35-40 vol.%), Pl (25-20 vol.%), Bt (15-20 vol.%), Hbl (10-8 vol.%), Grt (9-6 vol.%), Ilm (4-3 vol.%), Ep (2-3 vol.%), Ser, Chl (< 1 vol.%). Apatite, allanite-(Ce), rutile, and magnetite are present as accessories. The rock shows the crenulated structure and a porphyroblastic texture due to crystallization of coarse (at least 3-4 mm) garnet and smaller (up to 1-2 mm) plagioclase in the fine-grained matrix. The crenulated structure is formed by the presence of jet-like dark mineral aggregates surrounded porphyroblasts and lenticular clusters of granoblastic quartz grains (Fig.5, *a-c*).

Biotite occurs as part of these aggregates forming 0.3-0.4 mm thick plate crystals closely intergrown with coarser (1-2 mm) poikiloblastic amphibole (Fig.5, *d, e*). The matrix consists of plagioclase (fine poorly sericitized granoblastic grains with polysynthetic twins), epidote (prismatic crystals, up to 0.3-0.4 mm in size) and ilmenite (irregular grains, up to 0.1-0.2 mm in size).

Garnet forms poikiloblasts containing tails of quartz, ilmenite, and rutile grains; the two latter minerals are often intergrown (Fig.5, *f*). Garnet is corroded along grain boundaries and micro-fractures by late plagioclase, finely scaly biotite, chlorite, sericite, and ore minerals (Fig.5, *g*).

• Mineral chemistry. The composition of plagioclase is andesine to labradorite (An_{38-53}). Some crystals show patch zoning indicated by irregular areas composed of oligoclase (An_{24-26}). Amphibole is magnesio-tschermakite [20] with $Mg/(Mg + Fe^{2+})$ of 0.50-0.58 and TiO_2 content of 0.7-1.2 wt.%. Biotite typically contains moderate MgO (Mg# 0.49-0.51), low Al_2O_3 (15-16 wt.%, Al 1.35-1.45 apfu), and high TiO_2 (3-3.5 wt.%). The Fe^{3+} content in epidote is 0.50-0.56 apfu (O = 12.5). ΣREE concentration in allanite (Ce) is 0.7-1.1 apfu and Ce concentration is 0.34-0.46 apfu. Garnet is enriched in the grossular end member (X_{Ca} 0.18-0.21) and depleted in the spessartine end member (X_{Mn} 0.02-0.03). It shows X_{Mg} increase between core and rim from 0.10 to 0.16.

Mossel Series. Floen Suite. Metapelitic schist 3885-1

• Petrography. The rock contains Qz (25-30 vol.%), Ms (40-35 vol.%), Bt (15-20 vol.%), Grt (9-7 vol.%), Pl (8-5 vol.%), St (1-2 vol.%), Ilm (2-1 vol.%), Rt, Chl, carbonaceous matter (< 1 vol.%). Zircon, apatite, and monazite-(Ce) are present as accessories. The rock shows the crenulated structure formed by wave-curved aggregates of muscovite and biotite alternating with lenticular layers of quartz and plagioclase (Fig.6, *a*). The intergranular interstices of mica aggregates host plate ilmenite and rutile up to 100-150 μm lengthwise. The mineral typically present in the matrix is staurolite. It forms fine (< 0.1 mm) idiomorphic crystals of prismatic habit or clusters of grains oriented conformably with or at an angle to schistosity (Fig.6, *b*).

This is an open access article under the CC BY 4.0 license

© Yurii L. Gulbin, Sima A. Akbarpuran Khaiyati, Aleksandr N. Sirotkin, 2023

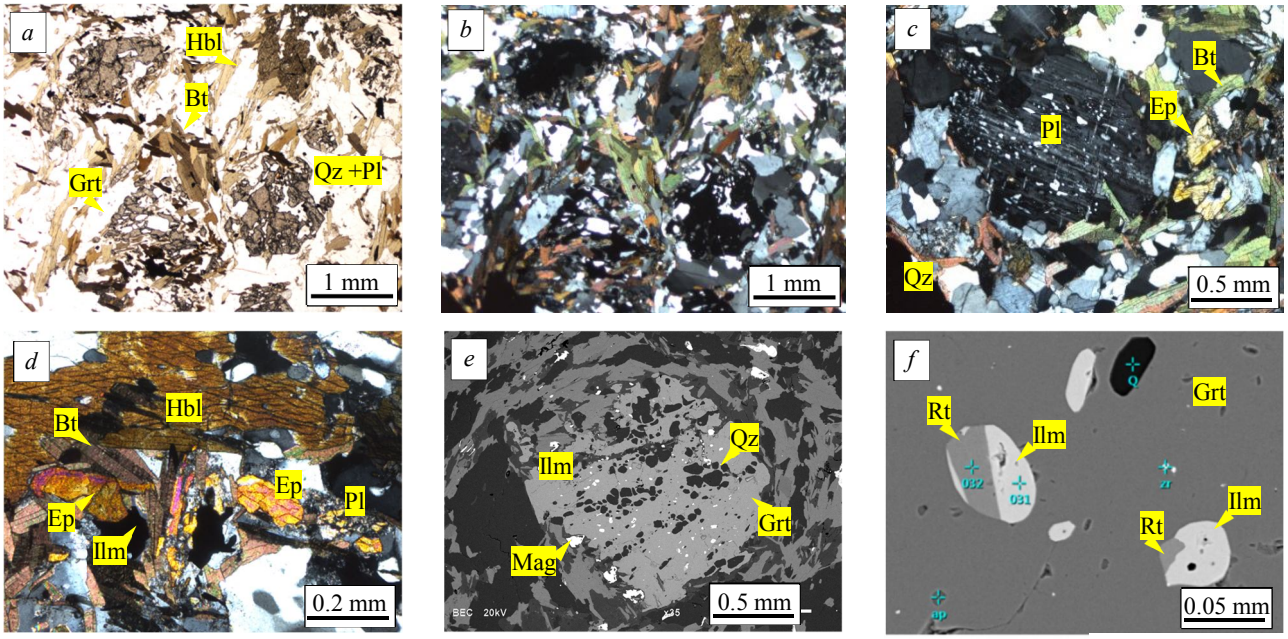


Fig.5. Mineral relationships in amphibole-biotite gneiss. Sample 4143-1. Images in transmitted light without analyzer (*a, g*), with analyzer (*b-d*) and in back-scattered electrons (*e, f*): *a, b* – garnet and amphibole porphyroblasts in quartz-plagioclase-biotite aggregate; *c* – plagioclase porphyroblast in quartz-plagioclase-epidote-biotite aggregate; *d* – epidote intergrown with amphibole and biotite; *e* – garnet porphyroblast with tails of quartz and ore mineral inclusions. Magnetite aggregates are confined to the lower rim of the porphyroblast; *f* – close-up of a fragment of rutile and ilmenite intergrowths in garnet (*e*); *g* – biotite-sericite-ilmenite veinlet cutting garnet

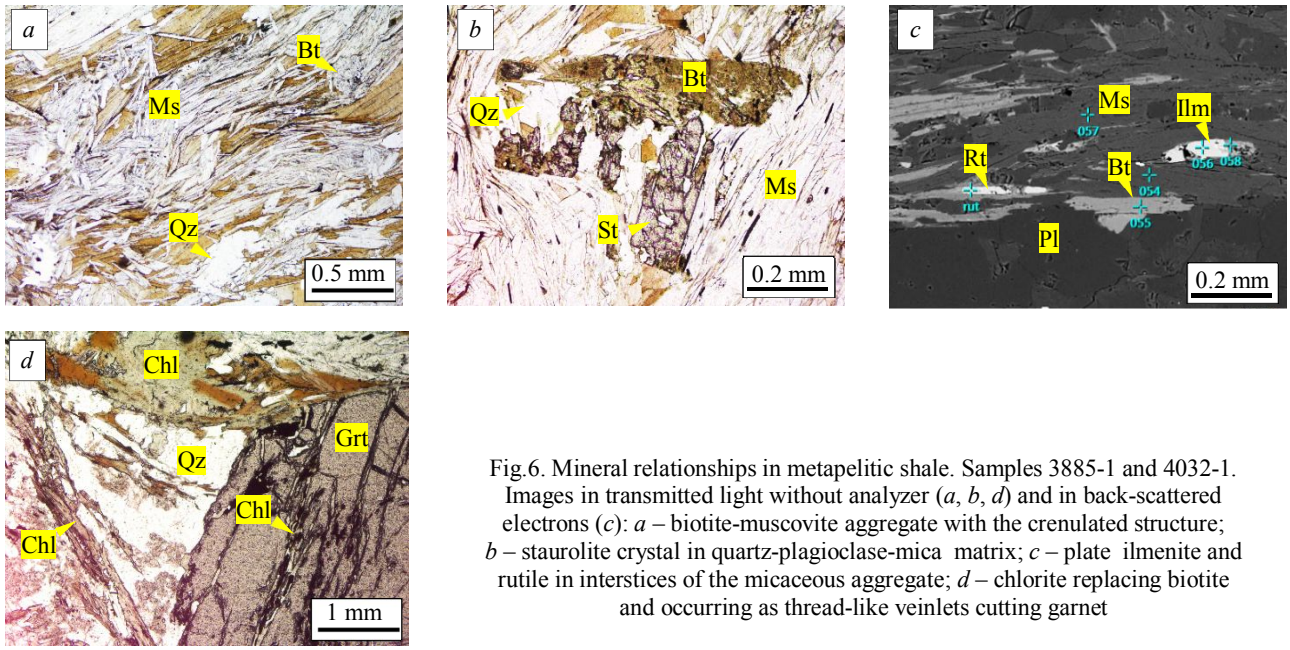


Fig.6. Mineral relationships in metapelitic shale. Samples 3885-1 and 4032-1. Images in transmitted light without analyzer (*a*, *b*, *d*) and in back-scattered electrons (*c*): *a* – biotite-muscovite aggregate with the crenulated structure; *b* – staurolite crystal in quartz-plagioclase-mica matrix; *c* – plate ilmenite and rutile in interstices of the micaceous aggregate; *d* – chlorite replacing biotite and occurring as thread-like veinlets cutting garnet

Micaceous aggregates surround coarse (up to 1 cm) garnet porphyroblasts included in a mantle of granoblastic quartz. An isometric shape of the porphyroblasts is often complicated because their branches are produced through the selective replacement of muscovite interlayers by garnet. The garnet is cut by chlorite micro-veinlets.

This is an open access article under the CC BY 4.0 license

Journal of Mining Institute. 2023. Vol. 263. P. 657-673
© Yurii L. Gulbin, Sima A. Akbarpuran Khaiyati, Aleksandr N. Sirotkin, 2023

• Mineral chemistry. Plagioclase is oligoclase (An_{14-15}) or less anorthitic (An_{2-4}) in late albitization zones. Muscovite is enriched in Na_2O (1.4-1.6 wt.%, Na 0.17-0.20 apfu), TiO_2 (0.27-0.30 wt.%), and SiO_2 (Si 3.11-3.14 apfu). Biotite contains moderate MgO (Mg# 0.52-0.53), elevated Al_2O_3 (19.4-20.4 wt.%), and low TiO_2 (1.5 wt.%). Staurolite is Fe-rich (Fe# 0.84) and contains minor ZnO (1.8 wt.%, Zn 0.38 apfu). Monazite (Ce 0.41-0.44 apfu) shows enrichment of ThO_2 (1.7-5.3 wt.%) and UO_2 (0.5-0.8 wt.%).

Garnet exhibits well-defined zoning due to core-rim depletion in X_{Mn} (in the range of 0.05-0.00) and enrichment in X_{Mg} (in the range of 0.04-0.15). Also the core of garnet porphyroblasts is more calcium (X_{Ca} 0.19-0.20) compared to the rim (X_{Ca} 0.05-0.06).

Mossel Series. Mosseldalen Suite. Metapelitic schist 4032-1

• Petrography. The rock contains Qz (35-40 vol.%), Ms (30-25 vol.%), Bt (22-20 vol.%), Grt (10-11 vol.%), Ilm (2-3 vol.%), Chl (1 vol.%), Rt (< 1 vol.%). Zircon, apatite, monazite-(Ce) and sulphides are present as accessories. The rock displays the crenulated structure and consists of lenticular interlayers of quartz and plagioclase alternating with jet-like aggregates of muscovite and biotite which surround coarse (up to 1 cm in size) garnet porphyroblasts. Interstices of the micaceous aggregate host numerous elongated ilmenite and rutile grains up to 50-100 μm in size (Fig.6, *c*). Chlorite locally replaces biotite.

Garnet porphyroblasts have idiomorphic or more complex *S*-shaped contours with tails of ilmenite and rutile inclusions, which inherit a schistosity pattern. Some of the porphyroblasts are overgrown with the quartz mantle; in this case, porphyroblasts have reticular rims instead of rectilinear boundaries. Additionally, in some places, garnet is cut by thread-like chlorite veinlets oriented at an angle to schistosity (Fig.6, *d*).

• Mineral chemistry. The plagioclase composition corresponds to oligoclase (An_{14-17}). It has been subjected locally to late albitization. Muscovite is enriched in Na_2O (1.6-2,1 wt.%, Na 0.18-0.25 apfu) and TiO_2 (0.21-0.41 wt.%) while it shows Si values between 3,01 and 3,12 apfu. Contents of celadonite and Fe-celadonite end members in white mica do not exceed 0.11 and 0.07 apfu, respectively. Biotite contains moderate MgO (Mg# 0.43-0.51), elevated Al_2O_3 (18.9-19.3 wt.%) and low TiO_2 (1.2-1.6 wt.%). Chlorite (ripidolite) exhibits enrichment in Fe (Fe# 0.47-0.70) and Al (2.5-2.7 apfu) and depletion in Si (2.6-2.8 apfu).

Garnet is enriched in the grossular end member (from core to rim, X_{Ca} ranges between 0.20-0.23 and 0.06-0.09). Simultaneously, garnet shows normal Mg and Mn zoning (core: X_{Mg} 0.03-0.04, X_{Mn} 0.03; rim: X_{Mg} 0.10, X_{Mn} < 0.01).

Ilmenite contains no more than 0.4 wt.% MnO. Monazite is characterized by the prevalence of Ce (0.40 apfu) over other rare earth elements (Nd 0.29, La 0.20, Pr 0.04, Sm 0.03 apfu) and contains 5.1 wt.% ThO_2.

Results of mineral thermobarometry.

• A garnet-biotite geothermometer, garnet-biotite-plagioclase-quartz, garnet-kyanite/sillimanite-quartz-plagioclase and garnet-rutile-ilmenite-plagioclase-quartz thermobarometers. For estimation of pressure and temperature at which minerals in metapelites and similar rocks were equilibrated, a geothermometer, based on an exchange reaction

$$Py + Ann = Alm + Phl\ (GB),$$

which describes the partitioning Fe and Mg between garnet and biotite when temperature rises, and thermobarometers, based on net transfer reactions

$$6An + 3Ann = Alm + Grs + 3Sid + Qz\ (GBPQ);$$

$$3An = Grs + 2\ Als + Qtz\ (GASP);$$

This is an open access article under the CC BY 4.0 license

$$3An + 6Ilm + 3Qz = 2Alm + Grs + 6Rt \text{ (GRIPS)},$$

which show the partitioning Ca between garnet and plagioclase when pressure rises, are widely used. Modern calibrations of these thermobarometers [21-23] are well-supported thermodynamically, based on experimental data and natural evidence, and take into account nonideality of garnet, biotite, and plagioclase solid solutions [24-26]. The application of the GASP geobarometer is limited by parageneses containing Al_2SiO_5 polymorphs and those of the GRIPS geobarometer by parageneses with ilmenite and rutile.

The garnet-biotite geothermometer showed that the peak metamorphic temperature of Atomfjella series metapelitic and calcic pelitic schists was 670-690 °C. Matrix biotite and rim of garnet with the highest MgO content were equilibrated at this temperature (Table 2). The pressure, calculated for this temperature with different thermobarometers, is variable. Higher pressure estimates (9.5-13.5 kbar) were obtained for the metapelitic schist and lower ones (7.2-8.2 kbar, GBPQ; 10.5-12 kbar, GRIPS) for calcic pelitic schists.

Table 2

Representative temperature and pressure estimates obtained with the garnet-biotite geothermometer and garnet-biotite-plagioclase-quartz (GBPQ), GASP, and GRIPS geobarometers

Sample	Analysis			Mole fractions								*T*, °C		*P*, kbar		
	Grt	Bt	Pl	X_{Ca}^{Grt}	X_{Mn}^{Grt}	X_{Mg}^{Grt}	X_{Ti}^{Bt}	X_{Al}^{Bt}	X_{Mg}^{Bt}	X_{Ca}^{Pl}	X_{Fe}^{Ilm}	GB_{KM04}	GB_{G10}	GBPQ	GASP	GRIPS
Atomfjella Series																
Metapelitic schist																
3912-3a	001	068	070	0.128	0.000	0.160	0.039	0.165	0.38	0.21	0.99	677	690	11.6	13.5	10.9
	013	005	008	0.091	0.000	0.154	0.051	0.128	0.38	0.21	0.99	667	673	9.5	11.5	10.2
Calcic pelitic schist																
3912-3b	034	069	070	0.270	0.045	0.096	0.057	0.083	0.47	0.82	0.88	609	601	8.2	–	10.5
4072-2	025	038	061	0.276	0.004	0.063	0.099	0.041	0.26	0.81	0.99	693	690	7.2	–	12.0
	028	006	079	0.312	0.004	0.057	0.083	0.058	0.28	0.49	0.99	676	676	8.2	–	11.2
Amphibole-biotite plagiogneiss																
4143-1	001	011	016	0.194	0.013	0.137	0.057	0.075	0.40	0.38	0.96	715	705	8.5	–	11.2
	084	046	047	0.170	0.013	0.158	0.058	0.056	0.45	0.32	0.96	708	692	9.4	–	10.9
	084	046	048	0.170	0.013	0.158	0.058	0.056	0.45	0.40	0.96	708	692	8.6	–	10.7
Mossel Series																
Metapelitic schist																
3885-1	001	063	050	0.048	0.000	0.146	0.028	0.165	0.42	0.15	0.98	580	590	7.6	8.8	11.3
	033	067	024	0.073	0.000	0.139	0.028	0.149	0.44	0.14	0.98	580	585	9.6	10.6	11.2
4032-1	001	034	037	0.140	0.001	0.087	0.024	0.167	0.40	0.14	0.99	555	560	10.6	–	9.4
	010	053	042	0.090	0.002	0.099	0.031	0.138	0.42	0.14	0.99	540	545	8.9	–	9.9
	025	032	014	0.075	0.002	0.115	0.024	0.139	0.38	0.16	0.99	600	605	9.5	–	9.9

Notes. Calibrations: garnet-biotite geothermometer [23] (GB_{KM04}), [24] (GB_{G10}); garnet-biotite-plagioclase-quartz geobarometer [25] (GBPQ), garnet-A_2SiO_5-plagioclase-quartz [22] (GASP) geobarometer, garnet-rutile-ilmenite-plagioclase-quartz [27] (GRIPS) geobarometer.

The peak metamorphic temperature for Mossel series metapelitic schists was 580-600 °C. Most of the pressure values obtained for this and lower temperatures reflecting mineral re-equilibration conditions at a retrograde stage (540-560 °C), were 9-11 kbar.

• Ti-in-biotite and Ti-in-muscovite geothermometers and the phengite thermobarometer. Two empirical geothermometers are based on temperature dependences of minor Ti in micas from metapelite [27, 28]. The peak metamorphic temperature calculated for the studied rocks with these geothermometers are similar to those obtained with the garnet-biotite geothermometer. They were 660-730 °C

This is an open access article under the CC BY 4.0 license

Journal of Mining Institute. 2023. Vol. 263. P. 657-673
© Yurii L. Gulbin, Sima A. Akbarpuran Khaiyati, Aleksandr N. Sirotkin, 2023

for the Atomfjella Series and 550-580 °C for the Mossel Series (Table 3). At these temperatures, Ti-rich micas in the matrix were crystallized. The overall spread of temperature estimates is much wider (Fig.7, *a*, *b*). With respect to biotite, decrease in calculated temperature (reaching tens of degrees) is typical for the mica crystals contacting with garnet and could be due to the partial loss of Ti provoked presumably by the exchange of femic components between two minerals at the retrograde stage. With respect to muscovite, such a decrease is most likely due to the presence of a low-temperature generation (< 500 °C) of white mica, which crystallized under greenschist facies conditions. It should be noted that the lowest temperature value (360 °C) calculated with the Ti-in-muscovite geothermometer (which was calibrated over the range 450-800 °C), is consistent with TiO_2 content of 0.13 wt.% close to the sensitivity threshold of the electron probe method (~0.1 wt.%). Because near one quarter of the white mica analyses have shown lower TiO_2 contents, no temperature estimates for them are available. This means that low-temperature white micas are more abundant than those shown on the histogram in Fig.7, *b*.

Table 3

Representative temperature and pressure estimates obtained with Ti-in-biotite geothermometer, Ti-in-muscovite geothermometer and phengite geobarometer

Sample	Analysis		Position	$Mg\#^{Bt}$	Crystallochemical coefficients (O = 11)						*T*, °C		*P*, kbar		
	Bt	Ms			Ti^{Bt}	Ti^{Ms}	Si^{Ms}	Al^{Ms}	Mg^{Ms}	Fe^{Ms}	B_{H05}	M_{WC15}	M_{MS87}	M_{CT08}	M_{K15}
Atomfjella Series															
Metapelitic schist															
3912-3a	077	076	m	0.48	0.172	0.037	3.17	2.58	0.157	0.090	677	650	7.1	11.1	9.7
	078	075	m	0.50	0.156	0.055	3.10	2.68	0.112	0.066	670	730	6.3	10.9	10.4
	068	066	c	0.48	0.112	0.025	3.04	2.83	0.078	0.069	605	565	3.0	2.4	6.2
Calcic pelitic schist															
3912-3b	024	077	m	0.39	0.200	0.007	3.10	2.79	0.074	0.015	690	370	2.3	–	1.2
	069	075	m	0.54	0.165	0.000	3.10	2.84	0.056	0.024	685	–	–	–	–
	022	–	c	0.41	0.053	–	–	–	–	–	360	–	–	–	–
4072-2	006	071	m	0.32	0.240	0.040	3.23	2.50	0.089	0.128	708	660	8.6	13.9	9.8
	038	062	m	0.31	0.280	0.000	3.14	2.78	0.000	0.043	728	–	–	–	–
Amphibole-biotite plagiogneiss															
4143-1	026	–	m	0.51	0.152	–	–	–	–	–	665	–	–	–	–
	086	–	m	0.50	0.200	–	–	–	–	–	705	–	–	–	–
Mossel Series															
Metapelitic schist															
3885-1	067	068	m	0.53	0.082	0.015	3.11	2.74	0.102	0.070	555	485	3.9	2.7	4.9
4032-1	053	046	m	0.51	0.090	0.025	3.05	2.81	0.073	0.062	570	555	3.3	2.7	5.8
	032	034	c	0.46	0.070	0.018	3.01	2.88	0.058	0.065	490	510	2.0	–	4.8

Notes. Calibration: Ti-in-biotite geothermometer [27] (B_{H05}); Ti-in-muscovite geothermometer [28] (M_{WC15}); phengite geobarometer [29, 30] (M_{MS87}), [31, equation 7] (M_{CT08}), [29, equation 4] (M_{K15}). Location of mica crystals: m – matrix, c – contact with garnet. $Mg\#^{Bt}$ = Mg/(Fe+Mg) in biotite.

Phengite thermobarometer takes into account the variations of Si, Fe, and Mg contents in white micas described by Tschermak's substitution $Al^{IV}Al^{VI} = Si + (Mg, Fe^{2+})$. Experiments [30] have shown that muscovite is enriched the high Si (celadonite) component in a low temperature and high pressure range. The thermobarometer equation based on these experiments was calibrated for the paragenesis of Ms-Phl-Kfs-Qz. When phengite mica is a part of other assemblages, this equation allows to estimate the lower limit of pressure [30]. More recent calibrations of the thermobarometer consider the results of the physical and chemical modeling of mineral parageneses in metapelites [31] and the results of the empirical generalization concerning temperature and pressure dependences of natural and synthetic phengite compositions [29].

This is an open access article under the CC BY 4.0 license

© Yurii L. Gulbin, Sima A. Akbarpuran Khaiyati, Aleksandr N. Sirotkin, 2023

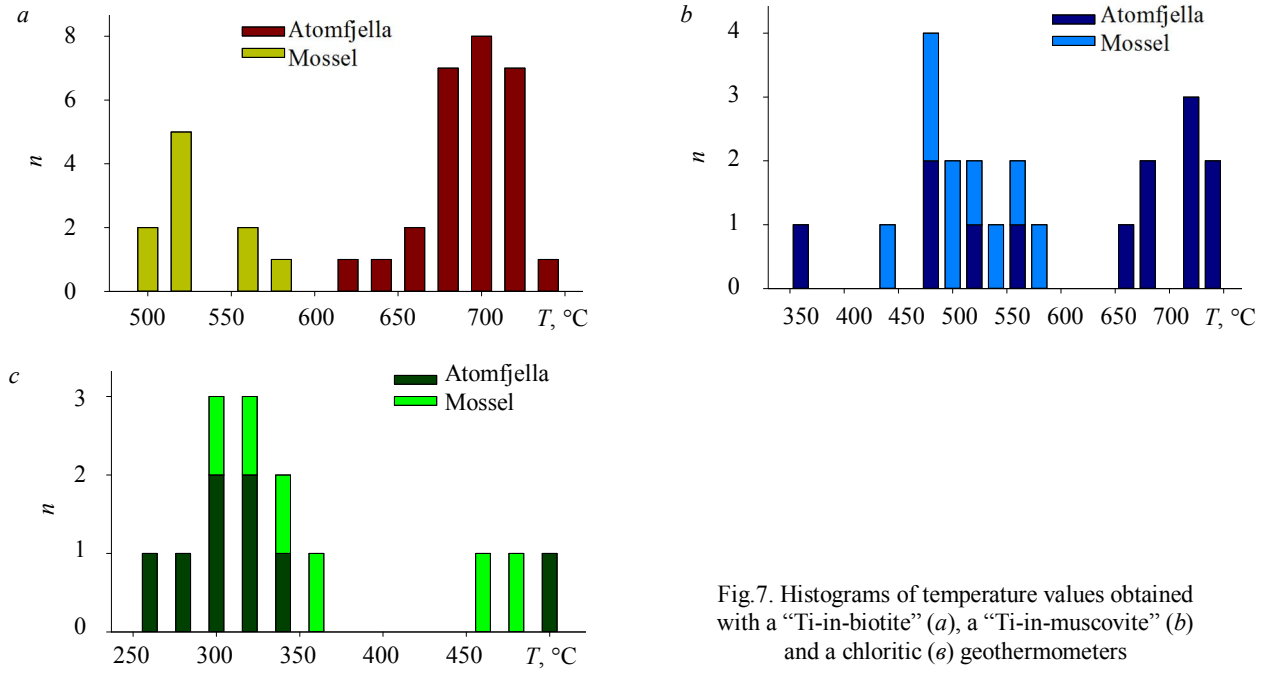


Fig.7. Histograms of temperature values obtained with a "Ti-in-biotite" (*a*), a "Ti-in-muscovite" (*b*) and a chloritic (*в*) geothermometers

For the peak temperatures calculated with the Ti-in-muscovite geothermometer, most of the pressure estimates obtained with the phengite thermobarometer for Atomfjella Series schists (Table 3) vary in the range of 6-8.5 kbar (M_{MS87}) or 9.5-11 kbar (M_{CT08}, M_{K15}). The latter result is in good agreement with the values obtained with the garnet-plagioclase thermobarometers (see Table 2). In the case of Mossel Series schists, similar values (3-6 kbar) were found to be underestimated. This could be due to the effect of more recent (relative to final stages of the porphyroblast formation) processes, which often contribute to the white mica recrystallization at low temperatures and pressures [30].

• Geothermometers and geobarometers considering variations in the calcium amphibole composition. An amphibole-plagioclase geothermometer, proposed for amphibolites and amphibole-biotite gneiss, is one of the more effective tool. It is based on a net transfer reaction which describes the appearance of increasingly aluminous amphibole in rocks containing quartz and plagioclase when temperature rises. Tschermak's substitution $^{A}\square + {}^{T1}Si = {}^{A}Na + {}^{T1}Al$, where □ is vacancy, is consistent with this reaction in the amphibole structure. The geothermometer equation was calibrated on the base of experimental data and models deal with nonideality of amphibole and plagioclase solid solutions [32]. The calculated temperatures, at which hornblende and plagioclase were equilibrated in the studied am-phibole-biotite gneiss sample (695-745 °C, Table 4), are stable and may be accepted as peak values.

Table 4

Results of thermobarometry of amphibole-biotite gneiss (sample 4143-1) obtained using calcium amphibole composition

Analysis			Crystallochemical coefficients in the amphibole (O = 23)									*T*, °C			*P*, kbar	
Hbl	Grt	Pl	Al^{T1}	Al^{M2}	Ti	Fe^{3+}	Fe^{2+}	Mg	Na^{M4}	Na^{A}	K	HP^{*}_{BH94}	GH^{**}_{GP84}	HP_{L21}	HP^{*}_{M15}	GHPQ**
041	071	016	1.75	0.67	0.093	0.83	1.25	2.13	0.179	0.135	0.110	695	620	665	8.5	8.3
042	084	047	1.92	0.66	0.105	0.64	1.63	1.94	0.019	0.289	0.138	745	660	690	9.3	8.2
043	071	047	1.75	0.64	0.097	0.65	1.54	2.07	0.015	0.261	0.163	712	640	675	8.9	9.2
101	071	047	1.91	0.67	0.131	0.70	1.46	1.99	0.104	0.219	0.161	725	645	725	8.9	9.6
102	071	016	1.79	0.72	0.078	0.59	1.79	1.80	0.0544	0.215	0.162	720	695	640	9.5	8.7

Notes. Calibrations: amphibole-plagioclase geothermometer [32] (HP_{BH94}); garnet-amphibole geothermometer [33] (GH_{GP84}); Ti-in-amphibole geothermometer [34] (HP_{L21}); amphibole-plagioclase thermobarometer [35] (HP_{M15}), garnet-amphibole-plagioclase-quartz thermobarometer [36] (GHPQ). Crystallochemical coefficients were calculated using the structural formula of amphibole $A(M_4)_2(M1_3)_3(M_2)_2(T_2)_4(T1)_4O_{22}(O,OH,F)_2$ [20]. Symbols * and ** show thermobarometers for which pressure and temperature estimates are mutually conformable.

This is an open access article under the CC BY 4.0 license

Journal of Mining Institute. 2023. Vol. 263. P. 657-673
© Yurii L. Gulbin, Sima A. Akbarpuran Khaiyati, Aleksandr N. Sirotkin, 2023

An amphibole-plagioclase thermobarometer [35] based approximately on the same grounds as the amphibole-plagioclase geothermometer. Being empirical, it takes into account the pressure-dependent variations of Al/Si ratio in amphibole and coexisting plagioclase. Pressure calculated with this thermobarometer and matched to temperatures calculated with the amphibole-plagioclase geothermometer was 8.5-9.5 kbar.

One of the major minerals present in amphibolite and amphibole-biotite gneiss is garnet. Therefore, thermobarometry of such rocks can also be performed with a garnet-amphibole geothermometer based on the exchange of Fe and Mg between garnet and hornblende, and with a garnet-amphibole-plagioclase-quartz thermobarometer based on a net transfer reaction, during which (while pressure rises) plagioclase is replaced by grossular garnet and released Al incorporates in amphibole. The equations for the thermobarometers were calibrated using metabasic rocks and take into account nonideality of mineral solid solutions [33, 36].

The equilibrium temperatures calculated with the garnet-amphibole geothermometer for the studied rock (620-660 °C in most cases) are much lower than peak temperatures. This discrepancy is probably due to the fact that Fe and Mg are more mobile than Al in the amphibole structure at low temperatures. This assumption is indirectly supported by the temperatures derived from a recently proposed empirical Ti-in-amphibole geothermometer [34]. Although the highest temperatures calculated with this geothermometer are close to peak values (690-725 °C), another part of temperature estimates in the range of 640-675 °C could be accepted as an evidence for the partial loss of relatively mobile Ti by amphibole when temperature falls.

Pressure calculated with the garnet-amphibole-plagioclase-quartz thermobarometer are the same as those calculated with the amphibole-plagioclase thermobarometer (8.5-9.5 kbar). It is noteworthy that peak temperature and pressure estimates obtained with thermobarometers taking into account variations in the composition of calcium amphibole agree well with those obtained with garnet-biotite and Ti-in-biotite geothermometers, as well as GBPQ and GRIPS thermobarometers (see Table 2 and 3).

Table 5

Representative compositions of chlorites and the results of chlorite geothermometry, wt.%

Series	Atomfjella				Mossel			
Sample	3912-3a	3912-3b			3885-1		4032-1	
Analysis	021	037	048	053	026	027	045	058
SiO_2	23.12	26.44	26.33	23.56	24.58	25.70	24.41	25.37
TiO2	0.00	0.00	0.00	0.00	0.00	0.24	0.00	0.00
Al_2O_3	19.70	18.96	17.32	20.96	19.92	21.95	21.98	20.72
FeO*	40.66	28.69	30.89	34.48	30.32	23.61	23.58	26.94
MnO	0.16	0.10	0.45	0.75	0.22	0.00	0.00	0.00
MgO	2.73	12.33	10.90	7.37	10.27	15.24	14.80	12.90
Sum	86.37	86.43	85.89	87.12	85.31	86.74	84.77	85.93
Crystallochemical coefficients (O = 14)								
Si	2.714	2.866	2.931	2.647	2.748	2.705	2.639	2.751
Al^{IV}	1.286	1.134	1.069	1.353	1.252	1.295	1.361	1.249
T	4.000	4.000	4.000	4.000	4.000	4.000	4.000	4.000
Al^{VI}	1.439	1.297	1.204	1.422	1.372	1.427	1.441	1.398
Fe	3.991	2.611	2.877	3.239	2.835	2.078	2.133	2.443
Mn	0.015	0.010	0.042	0.071	0.021	0.000	0.000	0.000
Mg	0.478	2.001	1.809	1.234	1.712	2.391	2.386	2.085
Sum	5.924	5.919	5.932	5.966	5.940	5.896	5.960	5.926
T, °C	335	268	249	492	353	319	466	325

Note. T – temperature calculated with a chlorite geothermometer [37].

This is an open access article under the CC BY 4.0 license

• Chlorite geothermometry. Empirically, it is based on the regular increase of Al^{IV} content in chlorite at rising temperature [37]. To approach this problem more rigorously, calibrations based on reactions involving both di- and tri-octahedral components of chlorite solid solutions should be used. One calibration considering the temperature dependence of the reaction $2Cln + 3Sud = 4Ame + 7SiO_2 + 4H_2O$ and assuming that $\Sigma Fe = Fe^{2+}$ [38] was used in the present study. Temperatures calculated with this geothermometer for studied rocks vary from 250 to 500 °C (Table 5). The distribution of temperature values is discrete: most of them range between 260-370 °C while minority of them range between 460-500 °C (Fig.7, *c*). The result obtained, together with the Ti-in-muscovite geothermometry data, indicate the presence of low-temperature chlorite and finely scaly muscovite (sericite) assemblage in the schists. This assemblage is a part of the late paragenesis Ms-Chl-Ep-Ab-Prh-Ttn that is characteristic of the low greenschist facies and the transition from greenschist- to prehnite-pumpellyite facies conditions.

Conclusion. As a result of the research, mineral composition and metamorphic conditions of rocks in Western Ny Friesland have been elucidated. Peak temperature and pressure during metamorphism of the Atomfjella Series were consistent with the high-pressure part of the upper amphibolite facies (690-720 °C, 9-12 kbar), while the same values of the Mossel Series were consistent with the high-pressure part of the lower amphibolite facies (580-600 °C, 9-11 kbar). In addition to the high-temperature parageneses Ms-Bt-Grt-Pl (±Ky, St), Bt-Grt-Pl-Kfs-Cal (±Scp), and Bt-Hbl-Ep-Grt-Pl, the rocks of both series host the low-temperature mineral assemblage Ms-Chl-Ep-Ab-Prh-Ttn which was formed upon transition from greenschist to prehnite-pumpellyite facies conditions (260-370 °C).

In contrast to the data reported by the earlier workers [14], our results were obtained with up-to-date mineral thermobarometers and take into account the maximum possible number of co-existing minerals. One of the main conclusions drawn from our study is that peak pressure obtained was higher than previously thought, which was achieved during the metamorphism of both series.

The authors are grateful to Candidate of Geological and Mineralogical Sciences, Senior Researcher O.L.Galankina (IPGG RAS) for her assistance in analytical studies.

REFERENCES

1. Ashikhmin D.S., Skublov S.G. Composition Heterogeneity of Xenoliths of Mantle Peridotites from Alkaline Basalts of the Sverre Volcano, the Svalbard Archipelago. *Journal of Mining Institute*. 2019. Vol. 239, p. 483-491 (in Russian). DOI: 10.31897/PMI.2019.5.483

2. Koreshkova M.Yu., Marin Yu.B., Nikitina L.P. et al. High-Alumina Pyroxenite Xenoliths from Quaternary Basalt of Spitsbergen Island: Evidence for Continental Crust Delamination. *Doklady Earth Sciences*. 2019. Vol. 485. N 5, p. 413-417. DOI: 10.1134/S1028334X19040123

3. Nikitina L.P., Marin Yu.B., Koreshkova M.Yu. et al. Xenoliths of High-Alumina Pyroxenites in the Basalts of the Sigurd Volcano, Spitsbergen Island (Svalbard Archipelago), as Indicators of the Paleozoic Geodynamics of the Regional Lithosphere. *Russian Geology and Geophysics*. 2022. Vol. 63. N 10, p. 1093-1110. DOI: 10.2113/RGG20214389

4. Egorov A.S., Prischepa O.M., Nefedov Y.V. et al. Deep Structure, Tectonics and Petroleum Potential of the Western Sector of the Russian Arctic. *Journal of Marine Science and Engineering*. 2021. Vol. 9. N 3, p. 1-26. DOI: 10.3390/jmse9030258

5. Kirsanova N., Lenkovets O., Hafeez M. Issue of Accumulation and Redistribution of Oil and Gas Rental Income in the Context of Exhaustible Natural Resources in Arctic Zone of Russian Federation. *Journal of Marine Science and Engineering*. 2020. Vol. 8. Iss. 12, p. 1-19. DOI: 10.3390/jmse8121006

6. Korago E.A., Kovaleva G.N., Schekoldin R.A. et al. Geological Structure of the Novaya Zemlya Archipelago (West of Russian Arctic) and Peculiarities of the Tectonics of the Eurasian Arctic. *Geotectonics*. 2022. Vol. 56, p. 123-156. DOI: 10.1134/S0016852122020030

7. Melnik A.E., Skublov S.G., Rubatto D. et al. Garnet and zircon geochronology of the Paleoproterozoic Kuru-Vaara eclogites, northern Belomorian Province, Fennoscandian Shield. *Precambrian Research*. 2021. Vol. 353. N 106014. DOI: 10.1016/j.precamres.2020.106014

8. Prischepa O., Nefedov Y., Nikiforova V. Arctic Shelf Oil and Gas Prospects from Lower-Middle Paleozoic Sediments of the Timan–Pechora Oil and Gas Province Based on the Results of a Regional Study. *Resources*. 2022. Vol. 11. Iss. 1. N 3. DOI: 10.3390/resources11010003

9. Vlasenko S.S., Sudarikov S.M. Ecological and hydrogeological state of oil and gas bearing areas of the Barents and Kara seas shelf. *Caspian Journal of Environmental Sciences*. 2021. Vol. 19. Iss. 3, p. 589-595. DOI: 10.22124/CJES.2021.4954

10. Gusev E.A., Krylov A.A., Urvantsev D.M. et al. Geological structure of the northern part of the Kara Shelf near the Severnaya Zemlya archipelago according to recent studies. *Journal of Mining Institute*. 2020. Vol. 245, p. 505-512. DOI: 10.31897/ PMI.2020.5.1

11. Bazarnik J., Barker A., Majka J. et al. Wstępna charakterystyka geochemiczna amfibolitów i skał ultramaficznych terrane West Ny-Friesland, północny Spitsbergen. *Przegląd Geologiczny*. 2021. Vol. 69. N 7, p. 406-410 (in Polish). DOI: 10.7306/2021.24

This is an open access article under the CC BY 4.0 license

12. Bazarnik J., Majka J., McClelland W.C. et al. U-Pb zircon dating of metaigneous rocks from the Nordbreen Nappe of Svalbard's Ny-Friesland suggests their affinity to Northeast Greenland. *Terra Nova*. 2019. Vol. 31. N 6, p. 518-526. DOI: 10.1111/ter.12422
13. Kośmińska K., Spear F.S., Majka J. et al. Deciphering late Devonian–early Carboniferous *P-T-t* path of mylonitized garnet-mica schists from Prins Karls Forland, Svalbard. *Journal of Metamorphic Geology*. 2020. Vol. 38, p. 471-453. DOI: 10.1111/jmg.12529
14. Sirotkin A.N., Evdokimov A.N. Endogenous regimes and evolution of regional metamorphism of folded complexes of the basement of the Spitsbergen archipelago (using the example of the Ny Friesland Peninsula). St. Petersburg: VNIIOkeangeologiya im I.S.Gramberga, 2011, p. 270 (in Russian).
15. *Whitney D.L., Evans B.W.* Abbreviations for names of rock-forming minerals. *American Mineralogist*. 2010. Vol. 95, p. 185-187. DOI: 10.2138/am.2010.3371
16. Akbarpuran Haiyati S.A., Gulbin Yu.L., Sirotkin A.N., Gembitskaya I.M. Compositional Evolution of REE- and Ti-Bearing Accessory Minerals in Metamorphic Schists of Atomfjellaa Series, Western Ny Friesland, Svalbard and Its Petrogenetic Significance. *Geology of Ore Deposits*. 2021. Vol. 63. N 7, p. 634-653. DOI: 10.1134/S1075701521070047
17. Keller L.M., De Capitani C., Abart R. A Quaternary Solution Model for White Micas Based on Natural Coexisting Phengite–Paragonite Pairs. *Journal of Petrology*. 2005. Vol. 46. Iss. 10, p. 2129-2144. DOI: 10.1093/petrology/egi050
18. Zolotarev A.A., Petrov T.G., Moshkin S.V. Peculiarities of chemical composition of the scapolite group minerals. *Geology of Ore Deposits*. 2003. Vol. 132. N 6, p. 63-84 (in Russian).
19. Holness M.B., Cesare B., Sawyer E.W. Melted Rocks under the Microscope: Microstructures and Their Interpretation. *Elements*. 2011. Vol. 7. N 4, p. 247-252. DOI: 10.2113/gselements.7.4.247
20. Leake B.E., Woolley A.R., Arps C.E.S. et al. Nomenclature of Amphiboles: Report of the Subcommittee on Amphiboles of the International Mineralogical Association, Commission on New Minerals and Minerals Names. *The Canadian Mineralogist*. 1997. Vol. 35. N 1, p. 219-246.
21. Holdaway M.J. Application of new experimental and garnet Margules data to the garnet-biotite geothermometer. *American Mineralogist*. 2000. Vol. 85. N 7-8, p. 881-892. DOI: 10.2138/am-2000-0701
22. Holdaway M.J. Recalibration of the GASP geobarometer in light of recent garnet and plagioclase activity models and versions of the garnet-biotite geothermometer. *American Mineralogist*. 2001. Vol. 86. N 10, p. 1117-1129. DOI: 10.2138/am-2001-1001
23. Kaneko Y., Miyano T. Recalibration of mutually consistent garnet-biotite and garnet-cordierite geothermometers. *Lithos*. 2004. Vol. 73, p. 255-269. DOI: 10.1016/j.lithos.2003.12.009
24. Gulbin Yu.L. Optimization of the Garnet–Biotite Geothermometer: Part II. Calibration Equations and Accuracy of the Estimation. *Geology of Ore Deposits*. 2011. Vol. 53. N 7, p. 543-557.
25. Wu Chun-Ming, Zhang Jian, Ren Liu-Dong. Empirical Garnet–Biotite–Plagioclase–Quartz (GBPQ) Geobarometry in Medium- to High-Grade Metapelites. *Journal of Petrology*. 2004. Vol. 45. Iss. 9, p. 1907-1921. DOI: 10.1093/petrology/egh038
26. Wu Meng-Chao, Zhao Guochun. The applicability of the GRIPS geobarometry in metapelitic assemblages. *Journal of Metamorphic Geology*. 2006. Vol. 24. Iss. 4, p. 297-307. DOI: 10.1111/j.1525-1314.2006.00638.x
27. Henry D.J., Guidotti C.V., Thomson J.A. The Ti-saturation surface for low-to-medium pressure metapelitic biotites: Implications for geothermometry and Ti-substitution mechanisms. *American Mineralogist*. 2005. Vol. 90, p. 316-328. DOI: 10.2138/am.2005.1498
28. Wu Chun-Ming, Chen Hong-Xu. Calibration of a Ti-in-muscovite geothermometer for ilmenite- and Al_2SiO_5-bearing metapelites. *Lithos*. 2015. Vol. 212-215, p. 122-127. DOI: 10.1016/j.lithos.2014.11.008
29. Kamzolkin V.A., Ivanov S.D., Konilov A.N. Empirical phengiticgeobarometer: substantiation, calibrationand practical application. *Geology of Ore Deposits*. 2015. Vol. 144. N 5, p. 1-14 (in Russian).
30. Massonne H.-J., Schreyer W. Phengite geobarometry based on the limiting assemblage with K-feldspar, phlogopite, and quartz. *Contributions to Mineralogy and Petrology*. 1987. Vol. 96, p. 212-224. DOI: 10.1007/BF00375235
31. Caddick M.J., Thompson A.B. Quantifying the tectono-metamorphic evolution of pelitic rocks from a wide range of tectonic settings: mineral compositions in equilibrium. *Contributions to Mineralogy and Petrology*. 2008. Vol. 156, p. 177-195. DOI: 10.1007/s00410-008-0280-6
32. Holland T., Blundy J. Non-ideal interactions in calcic amphiboles and their bearing on amphibole-plagioclase thermometry. *Contributions to Mineralogy and Petrology*. 1994. Vol. 116, p. 433-447. DOI: 10.1007/BF00310910
33. Graham C.M., Powell R. A garnet–hornblende geothermometer: calibration, testing and application to the Pelona Schist, Southern California. *Journal of Metamorphic Geology*. 1984. Vol. 2, p. 31-21. DOI: 10.1111/J.1525-1314.1984.TB00282.X
34. Liao Y., Wei C., Rehman H.U. Titanium in calcium amphibole: Behavior and thermometry. *American Mineralogist*. 2021. Vol. 106. N 2, p. 180-191. DOI: 10.2138/am-2020-7409
35. Molina J.F., Moreno J.A., Castro A. et al. Calcic amphibole thermobarometry in metamorphic and igneous rocks: New calibrations based on plagioclase/amphibole Al-Si partitioning and amphibole/liquid Mg partitioning. *Lithos*. 2015. Vol. 232, p. 286-305. DOI: 10.1016/j.lithos.2015.06.027
36. Kohn M.J., Spear F.S. Two new geobarometers for garnet amphibolites, with applications to southeastern Vermont. *American Mineralogist*. 1990. Vol. 75, p. 89-96.
37. De Caritat P., Hutcheon I., Walshe J.L. Chlorite geothermometry: A review. *Clays Clay Miner*. 1993. Vol. 41, p. 219-239. DOI: 10.1346/CCMN.1993.0410210
38. Lanari P., Wagner T., Vidal O. A thermodynamic model for di-trioctahedral chlorite from experimental and natural data in the system MgO-FeO-Al_2O_3-SiO_2-H_2O: applications to *P-T* sections and geothermometry. *Contributions to Mineralogy and Petrology*. 2014. Vol. 167, p. 1-19. DOI: 10.1007/s00410-014-0968-8

Authors: **Yurii L. Gulbin,** *Doctor of Geological and Mineralogical Sciences, Head of Department, https://orcid.org/0000-0003-3631-6843* (*Empress Catherine II Saint Petersburg Mining University, Saint Petersburg, Russia*), **Sima A. Akbarpuran Khaiyati,** *Junior Researcher, Akbarpuran_KhS@pers.spmi.ru, https://orcid.org/0000-0002-6089-9658* (*Empress Catherine II Saint Petersburg Mining University, Saint Petersburg, Russia*), **Aleksandr N. Sirotkin,** *Doctor of Geological and Mineralogical Sciences, Head of Department, https://orcid.org/0000-0003-2433-3953* (*Russian Research Institute for Geology and Mineral Resources of the World Ocean named after I.S.Gramberg, Saint Petersburg, Russia*).

The authors declare no conflict of interests.

This is an open access article under the CC BY 4.0 license